Error-prone mammalian female meiosis from silencing the spindle assembly checkpoint without normal interkinetochore tension

Agnieszka Kolano[a,b], Stéphane Brunet[a,b], Alain D. Silk[c,d], Don W. Cleveland[d,1], and Marie-Hélène Verlhac[a,b,1]

[a]Centre Interdisciplinaire de Recherche en Biologie, Unité Mixte de Recherche-Centre National de la Recherche Scientifique 7241/Institut National de la Santé et de la Recherche Médicale U1050, Collège de France, 75005 Paris, France; [b]Memolife Laboratory of Excellence and Paris Science Lettre, 75005 Paris, France; [c]Knight Cancer Institute and Department of Dermatology, Oregon Health and Science University, Portland, OR 97239; and [d]Ludwig Institute for Cancer Research and Department of Cellular and Molecular Medicine, University of California at San Diego, La Jolla, CA 92093

Contributed by Don W. Cleveland, March 20, 2012 (sent for review January 7, 2012)

It is well established that chromosome segregation in female meiosis I (MI) is error-prone. The acentrosomal meiotic spindle poles do not have centrioles and are not anchored to the cortex via astral microtubules. By Cre recombinase-mediated removal in oocytes of the microtubule binding site of nuclear mitotic apparatus protein (NuMA), which is implicated in anchoring microtubules at poles, we determine that without functional NuMA, microtubules lose connection to MI spindle poles, resulting in highly disorganized early spindle assembly. Subsequently, very long spindles form with hyperfocused poles. The kinetochores of homologs make attachments to microtubules in these spindles but with reduced tension between them and accompanied by alignment defects. Despite this, the spindle assembly checkpoint is normally silenced and the advance to anaphase I and first polar body extrusion takes place without delay. Females without functional NuMA in oocytes are sterile, producing aneuploid eggs with altered chromosome number. These findings establish that in mammalian MI, the spindle assembly checkpoint is unable to sustain meiotic arrest in the presence of one or few misaligned and/or misattached kinetochores with reduced interkinetochore tension, thereby offering an explanation for why MI in mammals is so error-prone.

kinetochore tension | mouse

Accurate segregation of chromosomes during cell division requires the assembly of a bipolar microtubule spindle. In most animal cells, bipolar mitotic spindle formation relies on centrosomes acting as major microtubule organizing centers (MTOCs). At mitosis onset, duplicated centrosomes rapidly promote spindle bipolarization (1), defining spindle poles as well as the spindle axis along which chromosome attachment and segregation will take place (reviewed in 2). Most oocytes, by contrast, lose their centrioles during oogenesis, and therefore lack canonical centrosomes (reviewed in 3). Mammalian meiotic spindle poles are not anchored to the cell cortex via astral microtubules. However, robust kinetochore fibers and spindle poles are established late in meiosis I (MI) (4), raising the question of how acentrosomal spindle poles, microtubules, and kinetochores cooperate to enable proper chromosome attachment and segregation.

Errors in meiotic chromosome segregation lead to the formation of aneuploid eggs, greatly compromising further embryo development. MI in human females is error-prone and is a leading cause of spontaneous abortion and congenital defects (5). It is now generally accepted that the spindle assembly checkpoint (SAC), also known as the mitotic/meiotic checkpoint, acts during MI in mouse oocytes to ensure successful attachment of the kinetochores of homologous chromosomes (whereas the sister kinetochores on each duplicated chromosome attach to microtubules from the same spindle pole) (6–9).

The molecular switch that silences the female meiotic checkpoint, as well as its robustness to prevent premature anaphase I, is unresolved. Studies using oocytes from females lacking a key synaptonemal complex gene (*Scp3*) have shown that passage through MI can occur in the presence of a few univalent chromosomes (10). Suppressing meiotic recombination in mouse oocytes lacking Mhl1, a protein essential for meiotic recombination, leads to premature separation of most homologs and major abnormalities in meiotic spindle assembly accompanied by chronic SAC-dependent meiotic arrest (11) or delay (12), depending on the genetic background. Efforts in male meiosis in insects have established that despite attachment to spindle microtubules, a single unpaired homolog provokes chronic SAC-dependent meiotic arrest (13) that is overcome by application of mechanical tension to the kinetochore of the unpaired homolog. No study to date has directly addressed the consequences of perturbing spindle tension on MI progression and SAC silencing in oocytes.

Work performed in *Xenopus* egg extracts has shown that the nuclear mitotic apparatus protein (NuMA) and dynein participate in focusing microtubules at spindle poles and allow the tethering of centrosomes to spindle microtubules (14, 15). To perturb meiotic spindle structure in oocytes and development of tension between kinetochores of homologs after bioriented attachment, we have now exploited an allele of NuMA in which the exon encoding the microtubule binding domain is selectively deletable by the Cre recombinase (16). In somatic cells, when mitosis takes place in the presence of this mutated form of NuMA, centrosomes establish initially focused spindle poles; however, as mitosis progresses, centrosomes are ejected from poles and focusing is lost (16).

We now use selective inactivation of NuMA to demonstrate that oocytes mutant for NuMA uniformly become aneuploid; thus, females are sterile, establishing an essential role for NuMA in female meiosis. Moreover, without functional NuMA, kinetochores of homologous chromosomes in mammalian female MI make bioriented attachments to spindles without development of normal tension between kinetochores. We exploit this discovery to test whether SAC silencing at the kinetochore requires simple

Author contributions: A.K. and M.-H.V. designed research; A.K. and S.B. performed research; A.D.S. and D.W.C. contributed new reagents/analytic tools; A.K., S.B., D.W.C., and M.-H.V. analyzed data; and A.K., S.B., A.D.S., D.W.C., and M.-H.V. wrote the paper.

The authors declare no conflict of interest.

Freely available online through the PNAS open access option.

[1]To whom correspondence may be addressed. E-mail: dcleveland@ucsd.edu or marie-helene.verlhac@college-de-france.fr.

See Author Summary on page 10761 (volume 109, number 27).

This article contains supporting information online at www.pnas.org/lookup/suppl/doi:10.1073/pnas.1204686109/-/DCSupplemental.

microtubule attachment or subsequent development of normal levels of interkinetochore tension.

Results and Discussion

NuMA Activity in Oocytes Is Essential for Female Fertility. We first confirmed that NuMA was present in mouse oocytes (17). NuMA was diffusely positioned early in MI, but within 4 h of meiotic entry, it was concentrated at spindle poles concomitantly with their formation (Fig. 1*A*). At telophase, a proportion of NuMA localized to the cleavage furrow between the oocyte and the forming polar body (Fig. 1*A*, time point NEBD + 8 h, white arrowhead). To address the function of NuMA in acentriolar spindle assembly, we used a conditional "floxed" allele of NuMA in which exon 22, which encodes its microtubule binding domain, is deletable by action of Cre recombinase (16) (Fig. 1*B*). Oocyte-specific deletion of NuMA in exon 22 was produced in female mice (Fig. 1*C*) that carried one floxed NuMA allele, one NuMA allele constitutively deleted of exon 22, and the ZP3-Cre transgene (18), the last of which encodes Cre expression only within oocytes.

Oocytes derived from these mice (referred to hereafter as Δ*22* oocytes) were homozygous for the exon 22 deletion. In late MI, these Δ*22* oocytes exhibited significant reduction in NuMA localization at spindle poles compared with control oocytes (Fig. 1 *D*, white arrows, and *E*). Cortical cleavage furrow association of NuMA was not compromised, strongly arguing for a specific inhibition in Δ*22* oocytes of NuMA microtubule binding without interfering with other binding partners (Fig. 1*D*, white arrowheads). The fertility of Zp3-Cre^{+};NuMA$^{wt/wt}$ and Zp3-Cre^{+}; NuMA$^{flox/\Delta 22}$ males was comparable, with each producing a mean litter size of five to six pups when crossed to Cre-expressing NuMA heterozygous females (Fig. 1*F*). Similarly, Zp3-Cre^{+}; NuMA$^{wt/\Delta 22}$ females crossed to *wt* males also produced litters of approximately five pups (Fig. 1*F*). In contrast, Zp3-Cre^{+};

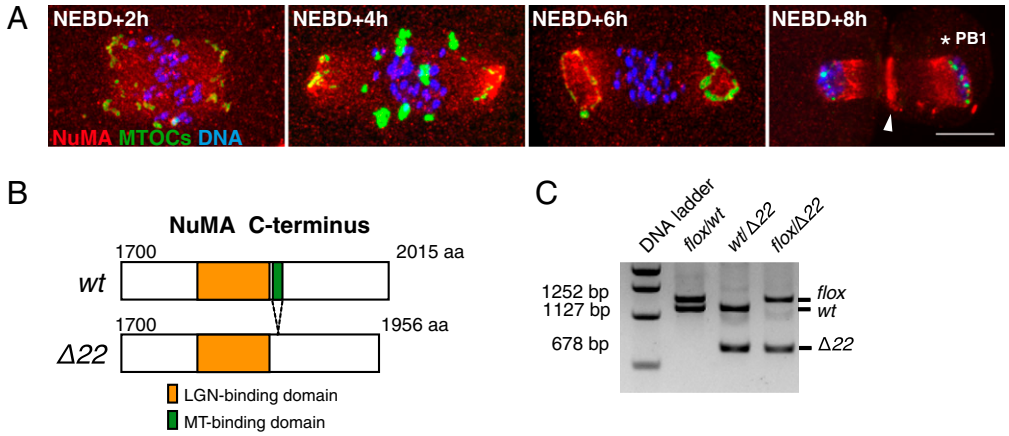

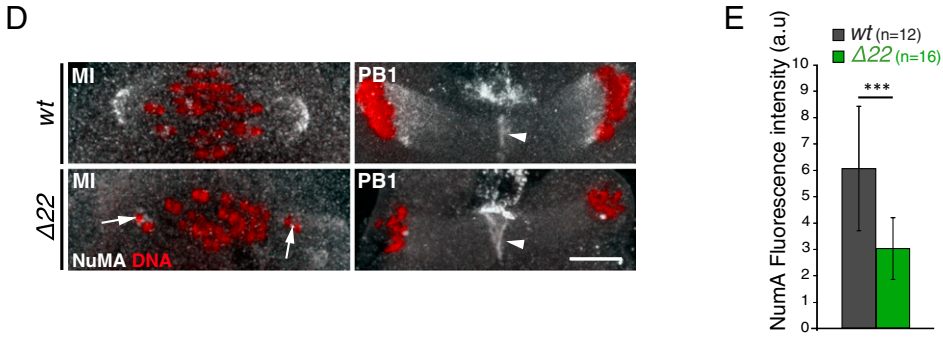

F

female	male	mean litter size
cre + ; NuMA *wt*/*flox* (or *wt*/Δ*22*)	cre + ; NuMA *wt*/*wt*	6 +/- 2.4
cre + ; NuMA *wt*/*flox*	cre + ; NuMA *flox*/Δ*22*	5.5 +/- 0.71
cre + ; NuMA *wt*/Δ*22*	cre + ; NuMA *flox*/Δ*22*	4.8 +/- 1.8
cre + ; NuMA *flox*/Δ*22*	cre + ; NuMA *flox*/Δ*22*	0

Fig. 1. NuMA is lost from spindle poles in the absence of its microtubule-binding domain. (*A*) NuMA and MTOCs accumulate at the spindle poles in MI. NuMA localizes to the cleavage furrow (white arrowhead) at PB1 (white star). Forty-nine oocytes were observed. (Scale bars: 10 μm unless otherwise specified.) (*B*) Scheme represents the deletion of the microtubule-binding domain of NuMA encoded by exon 22 in the mutant allele of NuMA (Δ*22*). (*C*) Genotyping of mice from crosses between the ZP3-Cre strain and the NumA$^{flox/flox}$ strain shows the efficiency of the Cre-recombinase to excise exon 22. Examples of *flox*/*wt*, *wt*/Δ*22*, and *flox*/Δ*22* genotypes are presented. (*D*) NuMA accumulation at spindle poles is reduced in Δ*22* oocytes (white arrows) compared with controls. NuMA remains associated with the cleavage furrow in Δ*22* oocytes (arrowheads). Nineteen oocytes were observed for controls, and 23 oocytes were observed for mutants. (*E*) Intensity of endogenous NuMA labeling was quantified and compared between control (gray) and Δ*22* (green) MI oocytes (***$P = 0.0002$). (*F*) Zp3-Cre^{+}; NuMA$^{flox/\Delta 22}$ females are sterile. The Zp3-Cre^{+}; NuMA$^{flox/\Delta 22}$ males are fertile when crossed with Cre^{+}; NuMA$^{wt/\Delta 22}$ or Cre^{+}; NuMA$^{wt/flox}$ females. Combinations of crosses and mean litter size (number of pups per cross) are indicated. At least three females were analyzed per cross for 6 mo after puberty.

NuMA$^{flox/\Delta 22}$ females, which produced oocytes homozygous for Δ*22*, were sterile; that is, they never gave rise to live pups (Fig. 1*F*), thereby demonstrating that NuMA and its microtubule binding are essential for female meiosis.

NuMA Is Required for Early Steps of Meiotic Spindle Assembly. To identify why loss of meiotic spindle-bound NuMA produced female sterility, the events of meiotic maturation were examined. The size and competence (oocytes need to reach a certain size during follicular growth to become competent to resume meiosis) of NuMA Δ*22* oocytes present in ovaries of sexually mature females were comparable to controls, demonstrating that follicular growth was not affected by ZP3-Cre–dependent homozygosity for NuMA Δ*22*. Indeed, when grown in culture, NuMA mutant oocytes initiated meiosis as efficiently as *wt* ones: 96% of Δ*22* oocytes initiated nuclear envelope breakdown (NEBD) vs. 93% of controls, and with normal kinetics (50% underwent NEBD within 30–45 min of transfer to culture medium). In addition, most NuMA-deficient oocytes extruded a first polar body (PB1) with normal kinetics (see Fig. 5 *A* and *B*).

Meiotic spindle assembly in the absence of functional NuMA was analyzed by time-lapse spinning disk microscopy using EB3-GFP, a (+)-end microtubule tracker, previously shown to track microtubule ends in mouse oocytes (4, 19). Following NEBD in *wt* oocytes, microtubules assembled between chromosomes and MTOCs formed the poles of bipolar spindles within ~3 h (Fig. 2 *A*–*C* and Movie S1). In contrast, Δ*22* oocytes exhibited impaired early steps of spindle assembly (Fig. 2*B* and Movie S2). After NEBD, chromosomes and microtubules were distributed over an area twice as large as in *wt* oocytes (Fig. 2 *B* and *D* and Movie S2). These enlarged spindles eventually bipolarized after a 1-h delay compared with control spindles (bipolarization at 4 ± 1 h in Δ*22* compared with 2 h 50 min ± 40 min in *wt*; $P = 0.003$; Fig. 2 *B* and *C*).

Four hours following NEBD, the resulting bipolar spindles were elongated (seen in live and fixed samples), with a twisted long axis and scattered chromosomes (Fig. 2 *B* and *E* and Movie S2). In addition, rather than the classic barrel shape characteristic of controls, the spindle poles were splayed (Fig. 2 *B* and *E*). Localization of hepatoma up-regulated protein (HURP), a marker of the central spindle domain (4, 20), was normal in the absence of microtubule-binding NuMA (Fig. S1*A*), whereas targeting protein for Xklp2 (TPX2), a marker of the peripolar domain, was abnormal, with its positioning spreading toward spindle extremities in the presence of NuMA Δ*22* (Fig. S1*B*).

In the absence of microtubule-bound NuMA, spindle poles underwent a surprising reorganization during MI. Whereas spindles maintained a stable barrel shape throughout the 8 h of MI in controls (Fig. 2*G* and Movie S3), they progressively closed to yield more focused poles before anaphase in NuMA Δ*22* oocytes (Fig. 2*G* and Movie S4). Astral-like structures were often observed at the extremities (Fig. 2*F*, arrowhead). Spindles of NuMA Δ*22* oocytes remained 40% longer than controls throughout all the latter stages of MI (Fig. 2*H*). This phenotype was maintained following PB1 extrusion for MII spindles, which elongated with hyperfocused poles (Fig. 2 *G* and *H*).

Meiotic Spindle Pole Shaping by NuMA Is a Two-Step Process. The formation of functional meiotic spindle poles in oocytes is divided into two phases. In the first, microtubules self-organize into a bipolar structure within the first hours of MI. Subsequently, components of the final MTOCs, originally scattered along the spindle axis, accumulate at spindle ends, where they organize and generate robust spindle poles (4). Our observations of aberrant spindle poles in the Δ*22* NuMA mutant oocytes, together with the known function of NuMA at spindle poles in mitotic cells (reviewed in 21), prompted us to analyze the nature of these meiotic defects more closely. To do this, we followed behavior of MTOCs by immunofluorescence analysis of pericentrin, a major MTOC component, and time-lapse microscopic analysis of Venus-tagged Polo kinase 1, which has previously been shown to associate with MTOCs in meiosis (22). Analysis of both time-lapse microscopy and fixed samples clearly showed that the kinetics of MTOCs sorting to the spindle poles were similar in control and mutant oocytes (Fig. 3 *A* and *C*). This result is consistent with previous findings that MTOC sorting depends on the presence of a central array of microtubules assembled by HURP and that HURP domain formation is not impaired in the absence of NuMA (Fig. S1*A*). Further, the amount of these MTOC components accumulated at the poles was comparable between controls and in the absence of microtubule-bound NuMA (Fig. 3*D*).

In contrast, the organization and final shape of MTOCs were strikingly different in the absence of NuMA binding to microtubules (Fig. 3*A*). Analysis of the circularity of individual MTOCs indicated that in controls, MTOCs formed large elongated structures (with a low index of circularity) circumscribing the poles. NuMA Δ*22* mutant oocytes exhibited mostly spherical MTOCs characterized by a circularity index close to 1 (Fig. 3 *A* and *E*), mimicking the shape of mitotic ones. Interestingly, these round MTOCs were poorly attached to spindle extremities and had a strong tendency to detach from spindle poles at the end of MI (Figs. 2*F* and 3*B*, arrowheads). NuMA is therefore required for proper organization of the polar domain of female mouse meiotic spindles.

NuMA-Dependent Meiotic Spindle Pole Organization Is Required for Efficient Chromosome Congression. To examine the role of NuMA-dependent organization of spindle poles in meiotic chromosome movement, chromosome congression toward the MI spindle center was assessed. In controls, chromosomes progressively aligned at metaphase, with anaphase I ensuing immediately following spindle migration to the cell cortex and with concomitant polar body extrusion (Fig. 2*G* and Movie S3). Analysis of live imaging of NuMA Δ*22* oocytes revealed that chromosomes were dispersed during early steps of MI, normal congression was impaired, and a tight metaphase alignment was never achieved (Fig. 2*G* and Movie S4). Quantitative analysis of chromosome congression using fixed samples confirmed these observations: although many chromosomes did congress towards the spindle center in NuMA Δ*22* mutants, close alignment of chromosomes was never achieved (Fig. 3*C*). In addition, at late MI, without microtubule-bound NuMA, one or more pairs of homologs frequently persisted at poles (Fig. 3*C*).

NuMA Is Required for Accurate Chromosome Segregation and Oocyte Euploidy. In *wt* oocytes, anaphase I takes place about 8–8.5 h after NEBD and after the last chromosome has aligned (Fig. 4*A* and Movie S5). In mutant oocytes, anaphase I also typically took place around 8–8.5 h after NEBD despite the presence of misaligned chromosomes (Fig. 4*A* and Movie S6). In addition, lagging chromosomes were often observed during anaphase (Fig. 4*A*, white arrows). Within the same NuMA Δ*22* spindle, chromosomes initially at or near spindle poles either became bioriented and congressed to metaphase (Fig. 4*B*, white arrow) or remained motionless at the poles for long periods (Fig. 4*B*, white asterisk).

Quantification of the chromosome number of MII oocytes showed that, as expected, most Δ*22* oocytes were aneuploid in contrast to control oocytes (80% compared with less than 20% in controls; Fig. 4 *C* and *D*). Chromosome abnormalities involved mostly the loss or gain of one or two chromosomes (Fig. 4*D*). These data show that proper assembly of spindle poles by NuMA is essential to support accurate chromosome congression and segregation in female meiosis, providing an explanation for female sterility in the absence of functional NuMA.

Anaphase Is Not Delayed Despite Chromosome Congression Defects in the Absence of Spindle-Bound NuMA. The previous observations unambiguously establish that without spindle-bound NuMA,

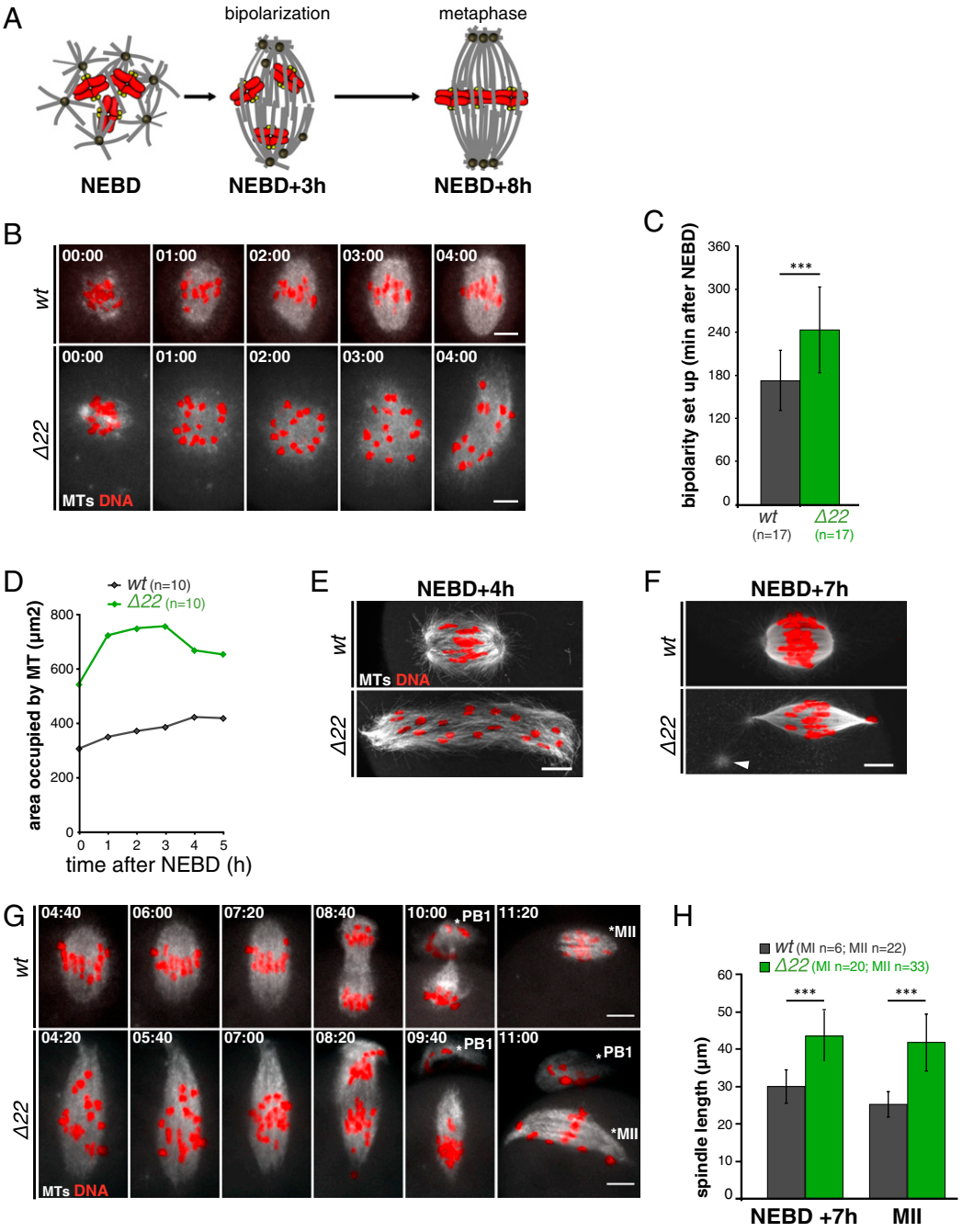

Fig. 2. NuMA is required for early MI spindle assembly. (*A*) Scheme represents the process of MI spindle assembly in control oocytes. After NEBD, bipolarization takes ~3 h. During the remaining 5 h before metaphase I, MTOCs are sorted and clustered to the poles, and bivalents biorient and congress to the equator. Bivalents are red with yellow kinetochores, microtubules are gray, and MTOCs are dark gray. (*B*) Mutant oocytes have defective early meiotic spindle assembly. NuMA is required to restrict the area of microtubule (MT) assembly at early steps: In the absence of functional NuMA, long MTs form, which organize slowly into roughly bipolar structures with unfocused poles. *wt* oocytes (n = 20; *Upper*); Δ*22* oocytes (n = 19; *Lower*). Oocytes express EB3-GFP (gray) and H2B-RFP (red). All times on all figures are hours and minutes after NEBD. (Scale bars: 10 μm unless otherwise specified.) (*C*) Histogram shows that the spindle bipolarization setup is delayed in Δ*22* oocytes. Bipolarity was scored when two poles were distinguishable. The mean time for Δ*22* oocytes is 288 ± 60 min (green) compared with 172 ± 40 min (gray) for *wt* oocytes (***P = 0.003). (*D*) Graph shows the surface occupied by MTs at early stages of MI spindle formation (*wt*, gray curve; Δ*22*, green curve). (*E*) Early defects result in long twisted spindles with broad poles and dispersed chromosomes, as observed on fixed oocytes at NEBD + 4 h. *wt* (n = 6; *Upper*); Δ*22* mutant (n = 6; *Lower*). (*F*) Metaphase I spindles in Δ*22* oocytes eventually resemble mitotic ones. They are elongated with hyperfocused poles presenting astral-like MTs (white arrowhead) not observed in controls, which are barrel-shaped. *wt* (n = 6; *Upper*); Δ*22* mutant (n = 20; *Lower*). (*G*) Spindle pole focusing during late stages of MI in mutant oocytes. Chromosome congress on a loose metaphase plate in Δ*22* (n = 30; *Lower*) compared with *wt* (n = 14; *Upper*) oocytes. Oocytes express EB3-GFP (gray) and H2B-RFP (red). The white star indicates the PB1. (*H*) Histogram of mean spindle length of MI and MII spindles from *wt* and Δ*22* oocytes. Mutant spindles (green) are 40% longer than controls (gray). The mean length of MI spindles in controls is 30.0 ± 4.5 μm and 43.6 ± 6.7 μm in Δ*22* (***P = 0.0001), and the mean length of MII spindles in *wt* is 25.1 ± 3.3 μm and 41.7 ± 7.6 μm in Δ*22* (***P < 0.001).

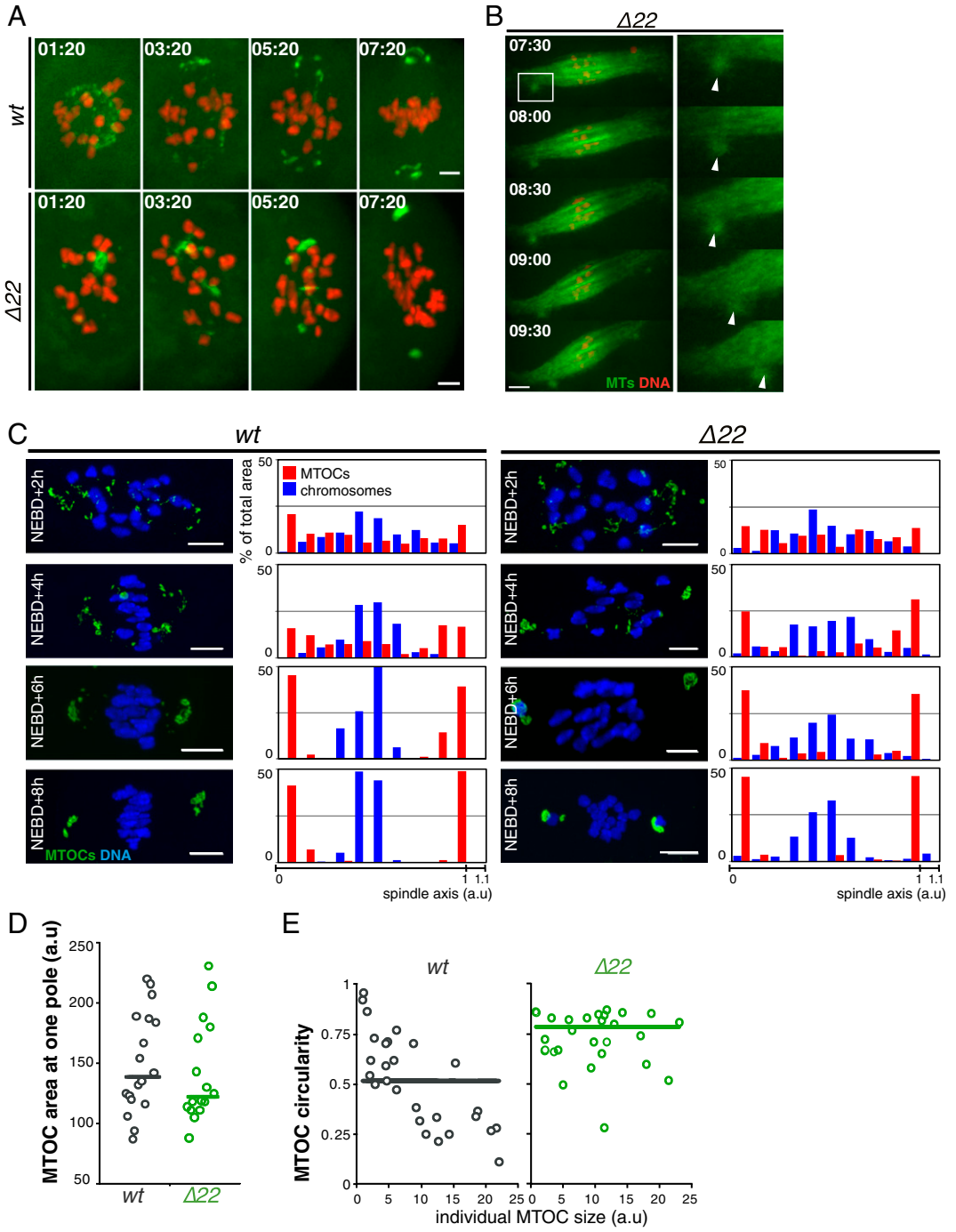

Fig. 3. NuMA is essential for the formation of meiotic barrel-shaped spindle poles. (*A*) MTOCs from mutant oocytes coalesce into a unique MTOC in MI. At the end of MI, MTOCs form structures made of discrete entities in *wt* oocytes ($n = 10$; *Upper*), whereas they appear compact in *Δ22* oocytes ($n = 18$; *Lower*), reflecting the morphology of poles. (Scale bars: 10 μm unless otherwise specified.) Oocytes express Venus-Plk1 (green) and H2B-RFP (red). (*B*) Large MTOC detaches from spindle microtubules (MTs) at the end of MI as observed in live mutant oocytes. Oocytes express EB3-GFP (green) and H2B-RFP (red). Smaller images (*Right*) correspond to a zoomed-in version of larger images (*Left*, *Inset*). The white arrowheads show an MTOC detaching from the spindle pole ($n = 20$ oocytes). (*C*) Kinetics of MTOCs sorting to the poles during MI are comparable in *wt* (*Left*) and *Δ22* (*Right*) oocytes, but chromosome congression is inefficient in mutants. Graphs show the quantitative analysis of MTOC distribution and chromosome congression along the spindle axis at 2 h (*wt*, $n = 8$; *Δ22*, $n = 7$), 4 h (*wt*, $n = 8$; *Δ22*, $n = 10$), 6 h (*wt*, $n = 9$; *Δ22*, $n = 14$), and 8 h (*wt*, $n = 10$; *Δ22*, $n = 12$) after NEBD. The graphs clearly show that chromosome congression is less efficient in mutants with few chromosomes stuck at spindle poles. (*D*) Mean area occupied by MTOCs at NEBD + 8 h in *Δ22* oocytes (green circles) is comparable to the area for *wt* oocytes (gray circles). Mutant oocytes do not lose MTOC material during their sorting to spindle poles. (*E*) Shape of MTOCs at NEBD + 8 h at the poles differs between *wt* and *Δ22* oocytes. The mean circularity shape factor is closer to 1 (with 1 corresponding to a perfect circle) in mutants (green circles) compared with controls (gray circles), showing that most MTOCs are circular in MI spindles, whereas controls have various shapes. a.u., arbitrary unit.

anaphase onset is triggered despite the continued presence of misaligned chromosomes resulting from defective spindle pole assembly. Indeed, counting of normal and NuMA *Δ22* oocytes revealed that 60% of mutant oocytes completed MI, extruding

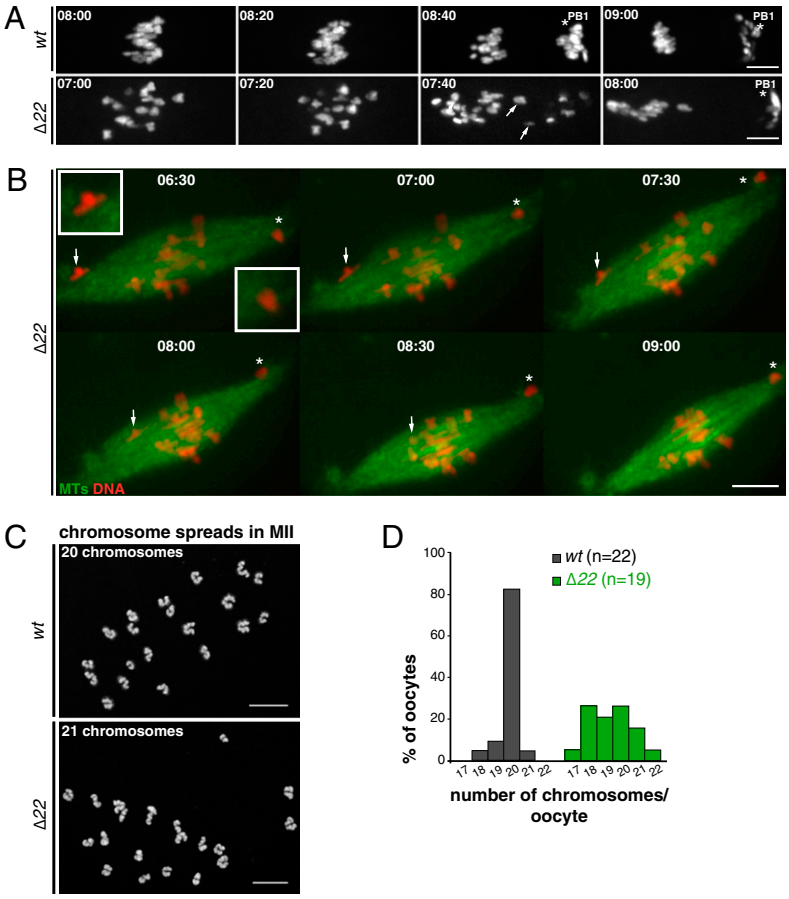

Fig. 4. NuMA is required for proper chromosome segregation. (*A*) Anaphase I in *wt* (n = 14; *Upper*) and Δ*22* (n = 30; *Lower*) oocytes expressing H2B-RFP. Lagging chromosomes are observed in mutants (white arrows). (Scale bars: 10 μm unless otherwise specified.) (*B*) Two different behaviors are shown on the same spindle for chromosomes lost at poles. One chromosome (*Left*; white arrow) is under tension, demonstrates bipolar attachment, and moves to the metaphase plate. The other chromosome (*Right*; white asterisk) stays at the pole. NuMA Δ*22* oocytes express EB3-GFP (green) and H2B-RFP (red). (*C*) Examples of chromosome spreads from MII *wt* (*Upper*) and Δ*22* (*Lower*) oocytes used to determine oocyte ploidy after the first meiotic division. Chromosomes are gray. Deconvolution was applied to images of chromosome spreads using Huygens Professional deconvolution software (SVI) to improve counting. (Scale bar: 5 μm). (*D*) Histograms represent the percentage of *wt* (gray) and Δ*22* (green) oocytes for each category of ploidy (17–22 chromosomes) determined by chromosome spreading as in *C*.

a PB1, compared with 79% of control oocytes. Very surprisingly, despite the presence of misaligned chromosomes whose kinetochores would have been predicted to continue to generate the "wait anaphase" SAC signal, polar body extrusion occurred without significant delay in oocytes without spindle-bound NuMA, yielding overall kinetics of polar body extrusion essentially indistinguishable from normal oocytes (Fig. 5*B*). Furthermore, kinetics of cyclin B1-GFP degradation were identical in normal and mutant oocytes (Fig. S2*A*), reinforcing the notion that progression to anaphase I was comparable with or without spindle-bound NuMA.

Robust SAC Signaling in Oocytes Depleted of Spindle-Bound NuMA. Prior work with preying mantid (13) and grasshopper (23, 24) spermatocytes had implicated the SAC in delaying meiotic anaphase until all chromosomes had stably attached to spindle microtubules and tension had developed between kinetochores of paired homologous chromosomes. Although many proteins involved in generation of the SAC signal are known (reviewed in 25) and no work in any system has implicated NuMA or a NuMA homolog as a component of the signaling pathway, the absence of MI delay in the NuMA Δ*22* oocytes called into question the robustness of SAC signaling in these oocytes. To examine SAC signaling more directly, low doses of nocodazole (100 nM), which have been shown to maintain an activated SAC and delay anaphase I onset (26), were added to normal and Δ*22* oocytes starting 6 h after NEBD. The ensuing disruption of spindle microtubule assembly continued activation of the SAC, which delayed polar body extrusion by 6 h in control oocytes (Fig. 5*C*). Similar treatment produced an even longer delay in polar body extrusion in oocytes without spindle-bound NuMA (Fig. 5*C*), consistent with nocodazole amplifying the spindle defects inherent to the Δ*22* mutant and demonstrating that the loss of spindle-bound NuMA (and presence of the Δ*22* protein) does not diminish SAC signaling or its sustained activation.

Further, we determined SAC signaling in Δ*22* oocytes following inhibition of Aurora B, a mitotic kinase whose activity is dispensable for nocodazole-mediated mitotic arrest by the SAC but necessary for sustaining taxol-dependent SAC activation (27, 28). Addition (to 100 nM) of the Aurora B inhibitor hesperadin to Δ*22* or normal oocytes at NEBD + 4 h (a time when Δ*22* oocytes are not yet bipolar) inhibited SAC signaling, advancing polar body extrusion in both oocyte genotypes (Fig. S2*B*). However, similar to what was seen in the case of nocodazole addition, SAC signaling was, if anything, enhanced in Δ*22* oocytes (i.e., it was sustained an additional hour compared with control oocytes). Lastly, we analyzed the effect of reversine, an inhibitor of the Mps1 kinase (29), whose activity is essential for

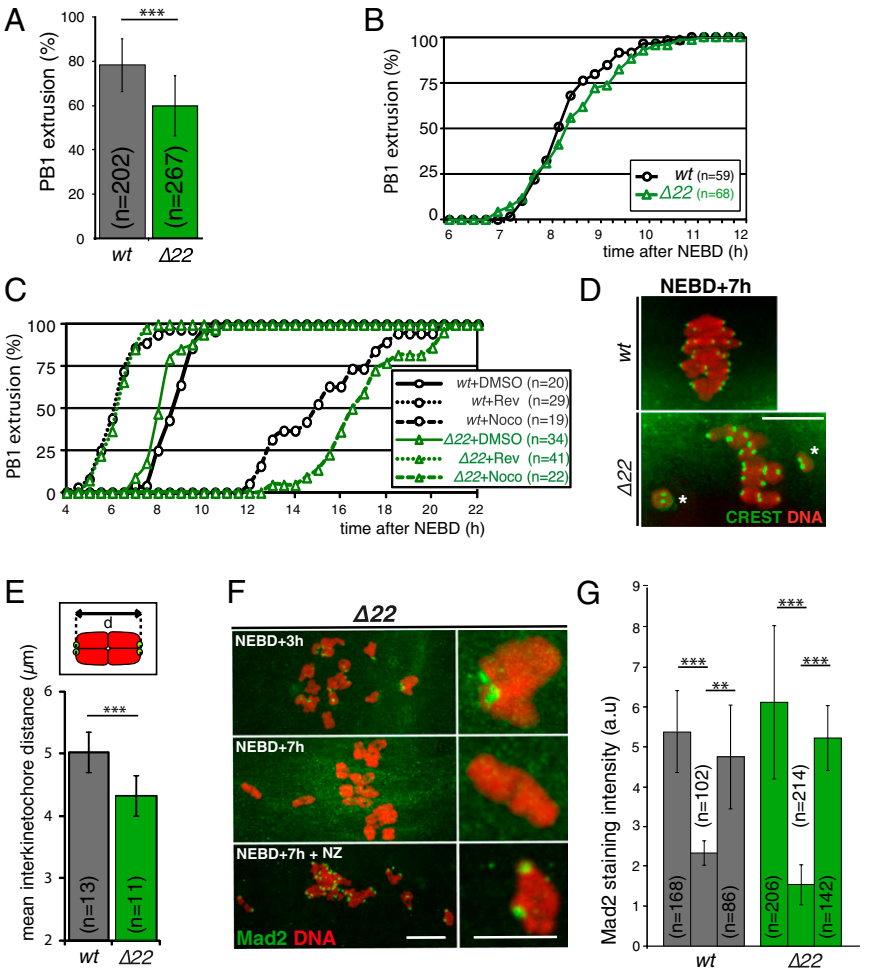

Fig. 5. SAC does not detect reduced tension on kinetochores in late MI. (*A*) Histogram represents the rate of PB1 extrusion in *wt* (gray) vs. Δ*22* (green) oocytes. Sixty percent of NuMA Δ*22* oocytes extrude PB1 compared with 79% in controls (***$P < 0.0001$). (*B*) Graph represents the kinetics of PB1 extrusion in *wt* (gray) vs. Δ*22* (green) oocytes. Mutant oocytes extrude PB1 with kinetics identical to controls: the mean time is 8 h and 30 ± 50 min for *wt* oocytes and 8 h and 40 min ± 1 h for Δ*22* oocytes ($P = 0.3$, not statistically significant). For all kinetics, the percentage of PB1 is calculated only from the population of oocytes extruding a polar body. (*C*) Graph represents the kinetics of PB1 extrusion in *wt* (gray) vs. Δ*22* (green) oocytes after treatment with reversine or with low doses of nocodazole. Reversine (100 nM) was added at NEBD, nocodazole (100 nM) was added at NEBD + 6 h, and oocytes were scored for PB1. Mutant oocytes respond to reversine like controls do: The mean time of PB1 is 6 h and 20 min ± 1 h and 10 min for *wt* oocytes (gray dotted line) and 6 h and 20 min ± 40 min for Δ*22* oocytes (green dotted line) treated with reversine and 8 h and 50 min ± 40 min for *wt* oocytes (gray solid line) and 8 h and 20 min ± 50 min for Δ*22* oocytes (green solid line) treated with DMSO. The difference in mean PB1 timing was extremely significant ($P < 0.0001$) between controls and reversine-treated oocytes. Mutant oocytes are also delayed after nocodazole treatment: The mean time of PB1 is 15 h and 20 min ± 2 h and 20 min for *wt* oocytes (gray broken line) and 16 h and 50 min ± 2 h for Δ*22* oocytes (green broken line) treated with nocodazole. The difference in mean PB1 timing was extremely significant ($P < 0.0001$) between controls and nocodazole-treated oocytes, and the difference between *wt* and Δ*22* oocytes treated with nocodazole was significant ($P = 0.0253$). (*D*) Representative images of metaphase I (NEBD + 7 h) plate from *wt* (*Upper*) vs. Δ22 (*Lower*) oocytes. Kinetochores are labeled with CREST (green). The white stars indicate unaligned chromosomes. (Scale bars: 10 μm unless otherwise specified.) (*E*) Quantification of interkinetochore distance from bivalents in oocytes as labeled in *D*. Tension exerted on kinetochores is reduced in Δ*22* oocytes: The mean value of the interkinetochore distance (d in the cartoon) for Δ*22* oocytes (green) is 4.4 ± 0.4 μm, and it is 5.0 ± 0.4 μm for *wt* oocytes (gray; ***$P = 0.001$). *n*, number of oocytes analyzed. For each oocyte, 20 interkinetochore distances were measured. (*F*) Mad2 is lost from all kinetochores, even unaligned ones, in Δ*22* oocytes (*Middle*) at NEBD + 7 h. Kinetochores in mutants are positive for Mad2 staining at NEBD + 3 h (*Top*) or at NEBD + 7 h after 30 min of treatment with 10 μM nocodazole (*Bottom*). (*Left*) Z-projections of confocal stacks. (*Right*) Magnifications of selected chromosomes. [Scale bar: 5 μm (*Right*).] (*G*) Quantification of Mad2 kinetochore labeling in *wt* (gray) vs. Δ*22* (green) oocytes at 3 h, 7 h post-NEDB, and 7 h post-NEBD after nocodazole treatment as in *F*. *n*, number of kinetochores observed. ** = 0.01; *** < 0.0001.

the SAC (29, 30). Treatment with reversine accelerated the metaphase I-to-anaphase I transition by 2–3 h similarly in both control oocytes, as previously reported (26), and Δ*22* oocytes (Fig. 5*C*), consistent with comparable SAC signaling in the two oocyte genotypes.

Taken together, these observations indicate that NuMA is not a component of SAC activity and that the SAC is fully active in NuMA Δ*22* oocytes. Consequently, the PB1 extrusion in the presence of misaligned chromosomes in Δ*22* oocytes is not attributable to an inherent inability to initiate or sustain SAC activation.

SAC Cannot Delay Anaphase I Despite Reduced Tension at Kinetochores. A widely accepted model is that in MI, the SAC wait anaphase signal is silenced by tension applied between the kinetochores of paired homologous chromosomes after attachment (13, 24; reviewed in 25, 31). Moreover, the lack of microtubule anchoring to the abnormal spindle poles in the absence of bound NuMA has been shown to reduce the tension applied to kinetochores in mammalian mitosis (16). We therefore determined interkinetochore tension in MI by measuring the distance between kinetochores in each bivalent after attachment

(Fig. 5*D*). Average interkinetochore distance was significantly reduced (from 5.0 ± 0.4 μm to 4.4 ± 0.4 μm) in NuMA Δ*22* vs. control oocytes (Fig. 5*E*). In the NuMA Δ*22* oocytes, the interkinetochore spacing on unaligned chromosomes near the poles was very significantly reduced (only 2.2 ± 0.9 μm), with spacing on some of these between 1 and 1.4 μm.

We could not accurately determine the distribution of interkinetochore distances for homologs under no tension, because microtubule assembly disruptors like nocodazole induce chromosome clumping that precludes a complete assessment. However, in the subset of chromosomes that were sufficiently separated from the others, interkinetochore distances of these presumptively unattached kinetochores were 1.3 ± 0.2 μm. Thus, not only were aligned chromosomes with bipolar attachments in the NuMA Δ*22* oocytes under reduced interkinetochore tension, but those at poles were under little, if any, tension.

HURP association onto kinetochores and microtubules at the end of MI enables visualization of K-fibers present in the oocyte (4). As expected, in control oocytes, chromosomes that had congressed to the equator of the spindle had HURP-decorated microtubules emanating from their kinetochores (Fig. S3). Similar figures were observed in NuMA Δ*22* oocytes, even for unaligned chromosomes located in the vicinity of the spindle poles (Fig. S3). Thus, the misorganization of spindle poles in mutant oocytes does not interfere with proper establishment of K-fibers.

Mad2 Disassociates from Kinetochores with Normal Kinetics Even with Reduced Tension. The spindle checkpoint component Mad2 localizes to unattached kinetochores (6) but is lost as stable kinetochore-microtubule interactions are established (6, 32) or in male meiosis after tension is applied (13, 23, 24). In both normal and NuMA Δ*22* oocytes, Mad2 was localized at kinetochores at NEBD + 3 h (Fig. 5 *F* and *G*). Subsequently, Mad2 staining disappeared, even from chromosomes that failed to achieve metaphase alignment in the NuMA Δ*22* oocytes (Fig. 5 *F* and *G*; NEBD + 7 h). Short treatment (30 min) of *wt* or NuMA mutant oocytes with 10 μM nocodazole induced the reappearance of Mad2 staining on kinetochores, demonstrating competency for checkpoint reactivation at unattached kinetochores (Fig. 5 *F* and *G*).

Thus, the SAC is normally activated and then satisfied at individual kinetochores in NuMA mutant oocytes, even in the presence of imperfectly aligned chromosomes near the spindle center and unaligned chromosomes whose kinetochores are under sharply reduced tension at poles. Some of these misaligned polar chromosomes are likely bioriented with reduced tension but with silenced SAC signaling. For others, with interkinetochore spacing similar to that in the absence of microtubules and more random orientations relative to the spindle axis than would be expected for correctly attached bivalents, these bivalents are unlikely to be attached in a bipolar manner. Rather, at least some of these are likely to be attached unstably or attached in an aberrant manner (e.g., with both kinetochores of a bivalent attached to microtubules from the most proximal pole so as to produce syntelic attachment). Nevertheless, SAC signaling is silenced, demonstrating that SAC satisfaction in this example of female meiosis in mammals is not mediated by development of normal interkinetochore tension.

NuMA-Dependent Spindle Pole Assembly in Meiosis. NuMA, together with dynein, anchors minus-ends of microtubules to the centrosomes of mitotic spindles. This function is not essential for early stages of mitotic spindle bipolarization, which is ensured by the two centrosomes, but becomes essential when robust bundles of kinetochore fibers form and transmit strong pulling forces between spindle poles and kinetochores. In the absence of functional NuMA, centrosomes are ejected from poles, poles splay open, and the equilibrium of forces essential for proper chromosome segregation is compromised. We show here that without centrosomes, NuMA is essential in the early stages of spindle assembly in mammalian meiosis. Our data establish that NuMA is required for shaping meiotic spindle poles, through activities that can be divided into two temporal phases. During the course of initial microtubule sorting into a bipolar array, at the time when MTOCs are dispersed along the spindle axis, NuMA ensures the cohesion of microtubule minus-ends and each of the two spindle poles. In the second phase of meiotic spindle formation, MTOCs are sorted toward these poles. During this phase, NuMA, probably with its partner dynein, acts as a microtubule spacer to maintain appropriate pole shape and allow deposition and further reorganization of MTOCs into the characteristic barrel shape of the meiotic spindle.

Strikingly, we have established that MTOC sorting to the poles takes place normally in the absence of functional NuMA. This can be explained by the fact that HURP, which is required to sort MTOCs to the poles, is appropriately localized to the central spindle region in NuMA-depleted oocyte spindles. Also noteworthy is that overexpression of lateral geniculate nucleus development (LGN), known to inhibit NuMA in mitosis (33, 34), induces spindle elongation and mitotic-like pole phenotypes that are strikingly similar to the ones we have observed using genetic NuMA disruption (35). This suggests that a correct balance of LGN and NuMA is required for proper organization of meiotic spindle poles.

Understanding the High Error Rate of Female Mammalian Meiosis. Evidence of missegregation in mouse MI of univalent, achiasmatic chromosomes after blocking almost all homologous recombination (by deletion of Mlh1) led Hunt and colleagues (12) to postulate that the oocyte SAC was unable to ensure stable bipolar attachment of bivalents before anaphase onset. Our evidence now demonstrates that the presence in mouse oocytes of poorly aligned chromosomes with sharply reduced interkinetochore tension does not delay, much less prevent, onset of meiotic anaphase I.

This outcome is strikingly different from the chronic delay seen in mouse oocytes with defective spindle architecture (4, 6, 12) and in insect spermatocytes (13, 23, 24). Indeed, efforts using micromanipulation of chromosomes in centriolar male meiosis in insects had initially concluded that tension generated by spindle forces between kinetochores of bivalents was required to silence SAC signaling by those kinetochores, thereby permitting advance to anaphase (12, 23). Additional efforts identified an interplay between microtubule attachment and tension, with increased tension stabilizing microtubule attachment (24, 36), and tension was again concluded to be essential for checkpoint silencing. Similarly, in maize meiosis, release of kinetochore-associated MAD2 is correlated with increased interkinetochore distance (i.e., tension) rather than initial attachment (37). In contrast to these examples, our evidence demonstrates that in mice, female MI is not delayed in response to reduced interkinetochore tension.

Most recently, it was proposed that the well-known high error rate of mammalian female meiosis is attributable to a high frequency of initial misattachment of kinetochores followed by incomplete error correction (38). This study neither followed chromosome movement into anaphase nor assessed SAC signaling. Although initial errors in attachment will produce an increased error frequency if uncorrected, our evidence demonstrates that a central determinant of a high error rate is that SAC signaling in mouse oocytes is silenced prematurely, even in the absence of spindle-induced tension and in the presence of multiple misaligned/misattached chromosomes. Moreover, our evidence establishes that even global reduction of tension on bivalent kinetochores (e.g., in NuMA-depleted spindles) is not

sufficient to delay anaphase, much less support sustained SAC signaling, producing anaphase initiation with normal kinetics and aneuploid oocytes instead. Thus, the SAC in mouse oocytes has a surprisingly low threshold for satisfaction and/or a poor signaling capacity. Recognizing this, our identification of an inherently weakened SAC that is silenced without normal tension, coupled with the initial errors of attachment (including merotelic and syntelic attachments) seen in an otherwise unperturbed meiosis (38), provides an explanation for why female MI in mammals is so error-prone.

Experimental Procedures

Mouse Strains and Genotyping. *Zp3-Cre* [C57BL/6-Tg(Zp3-cre)93Knw/J] breeding pairs were obtained from Jackson Laboratories. NuMA *flox/wt* mice were produced on a C57BL/6 background (16). For measurements of Cre-mediated NuMA exon 22 excision, genotyping was performed using the following primers: Cre 5′-GCG GTC TGG CAG TAA AAA CTA TC-3′ and 5′-GTG AAA CAG CAT TGC TGT CAC TT-3′, and NuMA 5′-AAC CGC ATC GCA GAG TTG CAG -3′ and 5′-GAG GAG TGG TGG CAA CAG TAG-3′.

Mouse Oocyte Collection and Culture. Oocytes were collected from 8- to 12-wk-old female mice into M2 + BSA medium supplemented with 150 μg/mL dibutyryl cAMP (dbcAMP; Sigma) to ensure a block in prophase I, as previously described (39). Resumption of meiosis was triggered by culturing oocytes in dbcAMP-free medium. All drugs were stored in DMSO at −20 °C and diluted in M2 + BSA. Nocodazole (Sigma) was used at 100 nM or 10 μM, reversine (Cayman Chemical Company) was used at 100 nM, and hesperadin (Calbiochem) was used at 100 nM as described by Kitajima et al. (38).

Plasmid Construction and in Vitro Transcription of cRNA. We used the following constructs: pRN3-histone-RFP (40), pRN3-EB3-GFP (19), and pRN3-cyclin B1-GFP (41). Plk1 (a gift from Erich Nigg, Biozentrum, Basel, Switzlerland) was subcloned into pSpe3-Venus (a gift from Alex McDougall, UMR 7009, Villefranche-sur-Mer, France). All cRNAs were synthesized using the T3 mMessage mMachine Kit (Ambion) and resuspended in RNase-free water as previously described (42).

Microinjection. Injection of in vitro-transcribed cRNAs into the cytoplasm of prophase I-arrested oocytes was performed using an Eppendorf Femtojet microinjector as described (43), and the oocytes were further kept for 2 h in dbcAMP arrest to allow expression of fusion proteins. Oocytes were then released from the prophase I stage by transferring and washing into dbcAMP-free M2 medium.

Live Imaging of Oocytes. Spinning disk movies were acquired using a Plan APO 40×/1.25 N.A. objective on a Leica DMI6000B microscope, enclosed in a thermostatic chamber set at 37 °C (Life Imaging Services), and equipped with a CoolSnap HQ2/CCD-camera (Princeton Instruments) coupled to a Sutter filter wheel (Roper Scientific) and a Yokogawa CSU-X1-M1 confocal scanner. MetaMorph software (Universal Imaging) was used to collect the data.

Chromosome Spreads. Chromosome spreads of metaphase II-arrested oocytes were prepared according to the method of Tarkowski (44) and stained with propidium iodide (5 mg/mL in PBS; Molecular Probes) for 20 min. Image acquisition was carried out on a Leica SP5/AOBS confocal microscope equipped with a Plan APO 100×/1.4 N.A. objective.

Immunofluorescence. Oocytes were prepared for fixation as described by Kubiak et al. (45). Microtubules were fixed with 0.1% glutaraldehyde as described by de Pennart et al. (46). For NuMA labeling, oocytes were fixed in ice-cold 100% methanol. For MTOC, TPX2, HURP, and CREST staining, 4% paraformaldehyde was used, and for Mad2 staining, 4% (vol/vol) formaldehyde (FA) with 0.15% Triton X-100 in Pipes Hepes EDTA Mops (PHEM) buffer was used as described by Wassmann et al. (6).

Rabbit polyclonal antibody against human NuMA (ab36999; Abcam) was used at a ratio of 1:100. Rat monoclonal antibody against tyrosinated α-tubulin (YL 1/2; Serotec) was used at a ratio of 1:200. Human α-CREST (HCT-100; Immunovision) was used at a ratio of 1:60. Mouse antipericentrin (BD Transduction Laboratories) was used at a ratio of 1:500. Rabbit–α-mHURP (sc-98809; Santa Cruz) was used at a ratio of 1:50. Rabbit α-human TPX2 (a gift from Oliver Grüss, ZMBH, Heidelberg, Germany) was used at a ratio of 1:500. Rabbit α-Mad2 (a gift from Katja Wassmann, UMR 7622, Paris, France) was used at a ratio of 1:200. As secondary antibodies, anti-rabbit Cy2 or Cy3, anti-mouse dye-light 488, anti-mouse Cy3, anti-rat Cy2 (all from Jackson Laboratories), and anti-human Alexa 488 (Molecular Probes) were used at a ratio of 1:200. Chromatin was stained for 20 min with Hoechst (5 μg/mL; Invitrogen) or propidium iodide (5 μg/mL; Molecular Probes). Citifluor AF-1 was used as a mounting medium.

Image acquisition of fixed oocytes was carried out on the SP5/AOBS confocal microscope equipped with a Plan APO 63×/1.4 N.A. objective.

Quantification Analysis. The measurement of NuMA fluorescence intensity at the poles in control and *Δ22* oocytes was performed on maximum projections of oocytes stained with NuMA using MetaMorph software. After background subtraction, two identical squares allowed us to measure the mean integrated intensity at poles.

The measurement of spindle length was performed using Volocity 4.1 software (Improvision) to obtain a 3D reconstruction of spindles after fixation (for this, we used the Z-stack acquired on the SP5/AOBS confocal microscope).

The measurement of interkinetochore distance was performed using Imaris software (Bitplans Scientific Software) on Z-stack images of oocytes stained with CREST.

The measurement of MTOC and chromosome distribution was performed using Z-projection of oocytes stained with pericentrin. For this purpose, we used ImageJ software (MacBiophotonics). The signals of chromosomes and pericentrin were binarized to assess the area of individual chromosomes or MTOCs (arbitrary units). The coordinates were then plotted along the spindle axis (0–1.1).

The measurement of cyclin B1-GFP fluorescence intensity was performed on maximum projections. After background subtraction, a circular frame with a diameter slightly smaller than the oocyte diameter allowed us to measure the maximum integrated fluorescence intensity within each cell. The cyclin B1-GFP intensity was measured inside this circular frame for all oocytes at recorded time points.

Normalization and correction were performed using Microsoft Excel software. Statistical analysis was performed using online GraphPad software.

ACKNOWLEDGMENTS. We thank Jérémie Teillon (Plate-Forme de Microscopie, Centre Interdisciplinaire de Recherche en Biologie) for his help with deconvolution of chromosome spreads. A.K. is a recipient of an Agence Nationale pour la Recherche postdoctoral fellowship (Grant ANR08-BLAN-0136-01 to M.-H.V.). S.B. is an Institut National de la Santé et de la Recherche Médicale fellow. This work was supported by Ligue Nationale Contre le Cancer Grant EL/2009/LNCC/MHV, Agence Nationale pour la Recherche Grant ANR08-BLAN-0136-01 (to M.-H.V.), and National Institutes of Health Grant GM 29513 (to D.W.C.).

1. Toso A, et al. (2009) Kinetochore-generated pushing forces separate centrosomes during bipolar spindle assembly. *J Cell Biol* 184:365–372.
2. Tanenbaum ME, Medema RH (2011) Mechanisms of centrosome separation and bipolar spindle assembly. *Dev Cell* 19:797–806.
3. Manandhar G, Schatten H, Sutovsky P (2005) Centrosome reduction during gametogenesis and its significance. *Biol Reprod* 72:2–13.
4. Breuer M, et al. (2010) HURP permits MTOC sorting for robust meiotic spindle bipolarity, similar to extra centrosome clustering in cancer cells. *J Cell Biol* 191: 1251–1260.
5. Hassold T, Hunt P (2001) To err (meiotically) is human: The genesis of human aneuploidy. *Nat Rev Genet* 2:280–291.
6. Wassmann K, Niault T, Maro B (2003) Metaphase I arrest upon activation of the Mad2-dependent spindle checkpoint in mouse oocytes. *Curr Biol* 13:1596–1608.
7. Homer HA, et al. (2005) Mad2 prevents aneuploidy and premature proteolysis of cyclin B and securin during meiosis I in mouse oocytes. *Genes Dev* 19:202–207.
8. Niault T, et al. (2007) Changing Mad2 levels affects chromosome segregation and spindle assembly checkpoint control in female mouse meiosis I. *PLoS ONE* 2:e1165.
9. McGuinness BE, et al. (2009) Regulation of APC/C activity in oocytes by a Bub1-dependent spindle assembly checkpoint. *Curr Biol* 19:369–380.
10. Kouznetsova A, Lister L, Nordenskjold M, Herbert M, Hoog C (2007) Bi-orientation of achiasmatic chromosomes in meiosis I oocytes contributes to aneuploidy in mice. *Nat Genet* 39:966–968.
11. Woods LM, et al. (1999) Chromosomal influence on meiotic spindle assembly: Abnormal meiosis I in female Mlh1 mutant mice. *J Cell Biol* 145:1395–1406.
12. Nagaoka SI, Hodges CA, Albertini DF, Hunt PA (2011) Oocyte-specific differences in cell-cycle control create an innate susceptibility to meiotic errors. *Curr Biol* 21: 651–657.
13. Li X, Nicklas RB (1997) Tension-sensitive kinetochore phosphorylation and the chromosome distribution checkpoint in praying mantid spermatocytes. *J Cell Sci* 110: 537–545.

14. Merdes A, Ramyar K, Vechio JD, Cleveland DW (1996) A complex of NuMA and cytoplasmic dynein is essential for mitotic spindle assembly. *Cell* 87:447–458.
15. Khodjakov A, Copenagle L, Gordon MB, Compton DA, Kapoor TM (2003) Minus-end capture of preformed kinetochore fibers contributes to spindle morphogenesis. *J Cell Biol* 160:671–683.
16. Silk AD, Holland AJ, Cleveland DW (2009) Requirements for NuMA in maintenance and establishment of mammalian spindle poles. *J Cell Biol* 184:677–690.
17. Tang CJ, Hu HM, Tang TK (2004) NuMA expression and function in mouse oocytes and early embryos. *J Biomed Sci* 11:370–376.
18. Lewandoski M, Wassarman KM, Martin GR (1997) Zp3-cre, a transgenic mouse line for the activation or inactivation of loxP-flanked target genes specifically in the female germ line. *Curr Biol* 7:148–151.
19. Schuh M, Ellenberg J (2007) Self-organization of MTOCs replaces centrosome function during acentrosomal spindle assembly in live mouse oocytes. *Cell* 130:484–498.
20. Yang G, Cameron LA, Maddox PS, Salmon ED, Danuser G (2008) Regional variation of microtubule flux reveals microtubule organization in the metaphase meiotic spindle. *J Cell Biol* 182:631–639.
21. Fant X, Merdes A, Haren L (2004) Cell and molecular biology of spindle poles and NuMA. *Int Rev Cytol* 238:1–57.
22. Pahlavan G, et al. (2000) Characterization of polo-like kinase 1 during meiotic maturation of the mouse oocyte. *Dev Biol* 220:392–400.
23. Li XT, Nicklas RB (1995) Mitotic forces control a cell-cycle checkpoint. *Nature* 373: 630–632.
24. Nicklas RB, Waters JC, Salmon ED, Ward SC (2001) Checkpoint signals in grasshopper meiosis are sensitive to microtubule attachment, but tension is still essential. *J Cell Sci* 114:4173–4183.
25. Musacchio A, Salmon ED (2007) The spindle-assembly checkpoint in space and time. *Nat Rev Mol Cell Biol* 8:379–393.
26. Hached K, et al. (2011) Mps1 at kinetochores is essential for female mouse meiosis I. *Development* 138:2261–2271.
27. Carvalho A, Carmena M, Sambade C, Earnshaw WC, Wheatley SP (2003) Survivin is required for stable checkpoint activation in taxol-treated HeLa cells. *J Cell Sci* 116: 2987–2998.
28. Hauf S, et al. (2003) The small molecule Hesperadin reveals a role for Aurora B in correcting kinetochore-microtubule attachment and in maintaining the spindle assembly checkpoint. *J Cell Biol* 161:281–294.
29. Santaguida S, Tighe A, D'Alise AM, Taylor SS, Musacchio A (2011) Dissecting the role of MPS1 in chromosome biorientation and the spindle checkpoint through the small molecule inhibitor reversine. *J Cell Biol* 190:73–87.
30. Perreira M, et al. (2005) "Reversine" and its 2-substituted adenine derivatives as potent and selective A3 adenosine receptor antagonists. *J Med Chem* 48:4910–4918.
31. Pinsky BA, Biggins S (2005) The spindle checkpoint: Tension versus attachment. *Trends Cell Biol* 15:486–493.
32. Brunet S, et al. (1999) Kinetochore fibers are not involved in the formation of the first meiotic spindle in mouse oocytes, but control the exit from the first meiotic M phase. *J Cell Biol* 146:1–11.
33. Du Q, Stukenberg PT, Macara IG (2001) A mammalian Partner of inscuteable binds NuMA and regulates mitotic spindle organization. *Nat Cell Biol* 3:1069–1075.
34. Du Q, Taylor L, Compton DA, Macara IG (2002) LGN blocks the ability of NuMA to bind and stabilize microtubules. A mechanism for mitotic spindle assembly regulation. *Curr Biol* 12:1928–1933.
35. Guo X, Gao S (2009) Pins homolog LGN regulates meiotic spindle organization in mouse oocytes. *Cell Res* 19:838–848.
36. King JM, Nicklas RB (2000) Tension on chromosomes increases the number of kinetochore microtubules but only within limits. *J Cell Sci* 113:3815–3823.
37. Yu HG, Muszynski MG, Kelly Dawe R (1999) The maize homologue of the cell cycle checkpoint protein MAD2 reveals kinetochore substructure and contrasting mitotic and meiotic localization patterns. *J Cell Biol* 145:425–435.
38. Kitajima TS, Ohsugi M, Ellenberg J (2011) Complete kinetochore tracking reveals error-prone homologous chromosome biorientation in mammalian oocytes. *Cell* 146: 1–14.
39. Terret M-E, et al. (2003) DOC1R: A MAP kinase substrate that control microtubule organization of metaphase II mouse oocytes. *Development* 130:5169–5177.
40. Tsurumi C, Hoffmann S, Geley S, Graeser R, Polanski Z (2004) The spindle assembly checkpoint is not essential for CSF arrest of mouse oocytes. *J Cell Biol* 167:1037–1050.
41. Ledan E, Polanski Z, Terret M-E, Maro B (2001) Meiotic maturation of the mouse oocyte requires an equilibrium between cyclin B synthesis and degradation. *Dev Biol* 232:400–413.
42. Verlhac MH, et al. (2000) Mos activates MAP kinase in mouse oocytes through two opposite pathways. *EMBO J* 19:6065–6074.
43. Verlhac M-H, Lefebvre C, Guillaud P, Rassinier P, Maro B (2000) Asymmetric division in mouse oocytes: With or without Mos. *Curr Biol* 10:1303–1306.
44. Tarkowski AK (1966) An air-drying method for chromosome preparation from mouse eggs. *Cytogenetics* 5:394–400.
45. Kubiak JZ, Weber M, Géraud G, Maro B (1992) Cell cycle modification during the transition between meiotic M-phases in mouse oocytes. *J Cell Sci* 102:457–467.
46. de Pennart H, Houliston E, Maro B (1988) Post-translational modifications of tubulin and the dynamics of microtubules in mouse oocytes and zygotes. *Biol Cell* 64:375–378.